ELSEVIER

Journal of Nuclear Materials 298 (2001) 321–328

journal of nuclear materials

www.elsevier.com/locate/jnucmat

Dependence of the non-swelling in-reactor steady-state creep component of austenitic phase alloys on the stacking fault energy

Edgar Robert Gilbert [1], John Paul Foster *

Commercial Nuclear Fuel Business Division, Westinghouse Electric Company, P.O. Drawer R, Columbia, SC 29250, USA

Received 7 November 2000; accepted 11 June 2001

Abstract

Steady-state irradiation creep data and stacking fault energy data are available for a wide composition range of austenitic phase alloys. The steady-state irradiation creep rate was found to increase with increasing stacking fault energy.

1. Introduction

The systematic variation of the steady-state irradiation creep rate, Bo, with SFE has apparently not been recognized because most investigators have been concerned with high dose (or swelling) effects. Further, variations in Bo can also mask the SFE dependence of Bo. Variations in calculated Bo appear to result from uncertainties in irradiation parameters, variabilities in creep data, and difficulties in separating the deformations associated with Bo from the dilations caused by phase changes and swelling phenomena. Garner [1] determined for 316 stainless steel that Bo ranged from $\sim$0.5 to $\sim 3 \times 10^{-6}$ MPa^{-1} dpa^{-1} with a nominal value of $\sim 1 \times 10^{-6}$ MPa^{-1} dpa^{-1}. Toloczko et al. [2] indicated that Bo may be mildly sensitive to alloy composition. Compositional effects on Bo have been somewhat obscured by the often larger strains that result from swelling and phase transformations. For example, Garner [1], Bates et al. [3] and Hausen and Schule [4,5] reported compositional effects on in-reactor deformation, but attributed most of the effect to volume changes resulting from solid-state phase transformations.

The low SFE of austenitic stainless steels causes Frank loops produced by irradiation to be split into sessile partial dislocations separated by stacking faults. Wolfer [6] reviewed irradiation creep theory and noted that a network of dislocations was produced by coalescence and unfaulting of the loops. Jitsukawa et al. [7] indicated that unfaulting during irradiation increases the creep rate. Jitsukawa et al. [8] attributed a complex response of irradiation creep by the climb/glide mechanism to the contraction of small loops resulting from the unfaulting of Frank loops and the increase in the number density of perfect loops. Where collapsed into jogged regions, these dislocations are able to climb and glide. Borodin and Ryazanov [9] indicate that both the non-swelling transient irradiation creep and the Bo irradiation creep compliance are sensitive to jog formation. The climb/glide mechanism for irradiation creep described by Stoller et al. [10] requires mobile dislocations for both transient and steady-state non-swelling creep. The configuration of the dislocations is also important in more recent creep models [11]. Unfaulting becomes more difficult with decreasing SFE. Therefore, alloy constituents that decrease the SFE should reduce the non-swelling creep compliance coefficient, Bo. The objective of this investigation is to determine the effect of composition and SFE on the non-swelling Bo irradiation creep compliance.

2. Irradiation enhanced deformation phenomena

The data analyzed by this investigation were selected so that swelling and phase transformations did not make

* Corresponding author. Tel.: +1-803 647 3632; fax: +1-803 695 4148.

E-mail address: fosterjp@westinghouse.com (J.P. Foster).

[1] Pacific Northwest National Laboratory, Richland, WA.

0022-3115/01/$ - see front matter
PII: S0022-3115(01)00646-8

large contributions to the strain. Deformation phenomena in austenitic stainless steels that are affected by irradiation include:

1. rapid deformation above the yield stress,
2. thermal creep,
3. non-swelling irradiation creep compliance (transient and steady state),
4. swelling-enhanced creep,
5. isotropic density changes from phase transformations,
6. isotropic stress-free swelling, and
7. stress-enhanced swelling.

This investigation is directed toward evaluating the effects of composition on the non-swelling steady-state irradiation creep rate. The influence of the other deformation phenomena was minimized by selecting tests conducted at stresses below the yield strength, neutron displacement damage levels below ~10 dpa, and temperatures within the range of ~300 °C to ~400 °C (note that strains associated with higher values of dose and temperatures tend to be dominated by swelling). The evaluation presented below will show that the Bo irradiation creep compliance is linearly dependent on the stacking fault energy. The linearity is described by the correlation coefficient, R^2. An R^2 value of 1.0 denotes perfect linearity. The effects listed above in general are not stacking fault energy dependent and therefore will decrease the correlation between Bo and the stacking fault energy (this decrease in correlation will be reflected by a decrease in R^2). These effects will decrease the value of R^2. The results of this investigation are not considered to be dominated by swelling because the effect of Ni on Bo was found to be opposite to the effect of Ni on swelling [12].

Garner [1] has described non-swelling irradiation creep rate using transient and steady-state terms. The formulation reported by Foster et al. [13] is

$$\mathrm{d}\varepsilon/\mathrm{d}t = (A_1 * A_2 * \exp(-A_2 * \varphi t) + \mathrm{Bo}) * \sigma, \tag{1}$$

where ε is the effective strain, t is time, A_1 is the amplitude of the transient component, A_2 describes the inverse of the period for transient (primary stage) creep term, Bo is the non-swelling steady-state creep compliance coefficient, σ is the effective stress and φt is the irradiation dose.

Values for A_1 are shown by Foster et al. [13] and by Garner [1] to range from 0 to $\sim 10 \times 10^{-6}$ MPa^{-1}. Experimental values for A_2 are shown by Foster et al. [13], to range from ~4 to 33 dpa^{-1}. A theoretical model described by Stoller et al. [10] indicates that the values of these creep coefficients have a complex dependence on stress, temperature, and atom displacement rate. The value of Bo is nominally $\sim 1 \times 10^{-6}$ MPa^{-1} dpa^{-1} [1] and ranges from ~0.5 to $\sim 3 \times 10^{-6}$ MPa^{-1} dpa^{-1}. The integrated form of Eq. (1) is

$$\varepsilon/\sigma = (A_1 * [1 - \exp(-A_2 * \varphi t)] + \mathrm{Bo}) * \varphi t. \tag{2}$$

The effective stress and strain are related to pressurized tube and spring stress and strain by the following relationships:

In the case of pressurized tubes:

$$\varepsilon = (2/1.73)\varepsilon_\theta,$$
$$\sigma = (1.73/2)\sigma_\theta,$$
$$\varepsilon/\sigma = (4/3)\varepsilon_\theta/\sigma_\theta.$$

In the case of springs:

$$\varepsilon = (1/1.73)\gamma,$$
$$\sigma = 1.73\tau,$$
$$\varepsilon/\sigma = (1/3)\gamma/\tau.$$

3. Data analysis

The SFE for austenitic stainless steels is reduced by decreasing Ni (for values <20 wt%), Al, Mn, C, and S; and by increasing Cr (for values <20 wt%), Mo, Si, N, Nb, Ti, and P [14–18]. The following correlation between SFE and composition was developed by Brofman and Ansell [14] from direct observation of dislocations:

$$\mathrm{SFE}\ (\mathrm{mJ/m^2}) = 16.7 + 2.1 * \mathrm{wt\%\ Ni} - 0.9 * \mathrm{wt\%\ Cr} + 26 * \mathrm{wt\%\ C}. \tag{3}$$

Other investigators have reported the SFE-composition dependence for Si, Mn, Nb, Ti, and N. The addition of Si over the range from 0.01 to 0.9 wt%, according to Table IX of Gallagher [16], reduces the SFE with a coefficient of −20.2 mJ/m^2/wt%. According to Li et al. [19], the composition coefficient for Mn is 0.21 mJ/m^2/wt%. The coefficients computed from Fig. 4 of Douglas et al. [18] were of the order of −8 to −11 mJ/m^2/wt% for Nb and Ti. Data in Fig. 9 of Swann [20] indicate that N significantly reduces the SFE. Schramm and Reed [15] determined a value of −77 mJ/m^2/wt% for the composition coefficient of N. While several investigators reported that Mo reduces the SFE, no quantitative correlations were found. Solutes that decrease the SFE also enhance the resistance to IGSCC [18] and pitting corrosion [21]. Therefore, the ratio of 3.3 reported for the composition coefficients of Mo and Cr for resistance to pitting corrosion and crevice corrosion, reported by Jargelius-Pettersson [22], was used for the Bo versus composition correlation. These results, in addition to Eq. (3), provided the following compilation of composition coefficients for SFE:

$$\begin{aligned}\text{SFE } (\text{mJ/m}^2) &= 16.7 + 2.1 * \text{wt\% Ni} - 0.9 * \text{wt\% Cr} \\ &\quad + 26 * \text{wt\% C} - 20.2 * \text{wt\% Si} \\ &\quad + 0.21 * \text{wt\% Mn} - 3 * \text{wt\% Mo} \\ &\quad - 8 * \text{wt\% Nb} - 11 * \text{wt\% Ti} - 77 * \text{wt\% N}. \end{aligned} \quad (4)$$

Eq. (4) was used to develop a preliminary correlation between the Bo coefficients for stainless steel pressurized tubes irradiated in five different nuclear reactors and the SFE calculated from the alloy compositions. Effective values of SFE during creep of stressed alloy test articles during neutron irradiation at elevated temperatures deviate from values of SFE measured during direct observation at ambient temperature. Therefore, values of the composition coefficients in Eq. (4) were varied slightly to increase the coefficient of correlation, R^2, for Bo versus SFE. The value of R^2 was further improved by adding composition terms for P, Cu, and S. Table 1 lists the values of Bo and the SFE. In addition, the results for the SFE and the correlation between Bo and the SFE (see Fig. 1) are

$$\begin{aligned}\text{SFE } (\text{mJ/m}^2) &= 19.5 + 2.6 * \text{wt\% Ni} - 0.9 * \text{wt\% Cr} \\ &\quad + 26 * \text{wt\% C} - 16.3 * \text{wt\% Si} \\ &\quad + 0.21 * \text{wt\% Mn} - 3 * \text{wt\% Mo} - 8 * \text{wt\% Nb} \\ &\quad - 11\text{wt\% Ti} - 77 * \text{wt\% N} - 20 * \text{wt\% P} \\ &\quad - 15 * \text{wt\% Cu} + 150 * \text{wt\% S}. \end{aligned} \quad (5)$$

$$\text{Bo } (10^{-6}\ \text{MPa}^{-1}\ \text{dpa}^{-1}) = 0.084 * \text{SFE } (\text{mJ/m}^2) - 0.80. \quad (6)$$

As indicated in Fig. 1, the correlation coefficient was 0.88.

To provide an independent validation of the correlation, a different set of in-reactor creep test data generated under a different stress state in a different nuclear reactor was evaluated. Garner and Toloczko [22] showed that the low-fluence, low-flux data reported by Lewthwaite and Mosedale [23] were still in the transient stage. Therefore, only the Bo coefficients reported for the higher-flux, higher-dose data which are in the steady-state irradiation creep range were used for the correlation of Bo with the SFE. The Half-Nelson a/a dose units were converted to dpa units using 100 Half-Nelson a/a per 85 dpa as described by Garner and Toloczko [22]. Table 2 lists the Bo and SFE values for helices tested in the DFR [23,24]. As with the pressurized tube data, the composition coefficients were adjusted within the range of values reported from direct observation to increase the coefficient of correlation. The results are (see Fig. 2)

$$\begin{aligned}\text{SFE } (\text{mJ/m}^2) &= 30 + 1.6 * \text{wt\% Ni} - 0.9 * \text{wt\% Cr} \\ &\quad + 26 * \text{wt\% C} - 16.3 * \text{wt\% Si} \\ &\quad + 0.21 * \text{wt\% Mn} - 3 * \text{wt\% Mo} - 0 * \text{wt\% Nb} \\ &\quad - 11 * \text{wt\% Ti} - 125 * \text{wt\% N} \\ &\quad - 80 * \text{wt\% P} - 0 * \text{wt\% Cu} + 175 * \text{wt\% S}, \end{aligned} \quad (7)$$

$$\text{Bo } (10^{-6}\ \text{MPa}^{-1}\ \text{dpa}^{-1}) = 0.21 * \text{SFE } (\text{mJ/m}^2) - 2.6, \quad (8)$$

The value of R^2 was 0.92. This independent set of data for a different stress state (torsion) in a single different reactor confirms that the SFE is an important parameter influencing the non-swelling irradiation creep compliance. Slight differences in the values of the composition coefficients resulted for the tests with pressurized tube and the tests with helices. These differences may be a result of incomplete reporting of solutes in the alloys, differences in solute concentrations, and uncertainties in Bo values. Improvement in the correlation requires systematic tests over a broad range of compositions and characterized test article microstructures.

4. Discussion

Additional evidence for a correlation between Bo and SFE is that the temperature dependencies of the Bo coefficient and the SFE are similar. An increase in temperature is associated with an increase in both Bo and the SFE. In the case of Bo, Wolfer [6], Woo and Garner [11], and Foster et al. [25] show that the value of Bo increases with increasing temperature over the range from ~200 °C to ~600 °C, with an unexplainable deviation of a high value of Bo at 300 °C shown in Fig. 11 of Foster et al. [25]. In the case of SFE, Latanision and Ruff [17] found the SFE for stainless steel containing 10.7 wt% Ni increased from an ambient temperature value of ~17 to ~31 mJ/m^2 at 325 °C. The increase in SFE with increasing temperature was much larger between ambient temperature and 135 °C than between 135 °C and 325 °C. According to the results reported by Latanision and Ruff [17], the effect of Ni on SFE is smaller over the temperature range from 300 °C to 400 °C than from ambient to 135 °C. Hence, the SFE was considered to be approximately constant for temperatures in the range of 250–400 °C (i.e., the temperature range of the irradiation creep tests). The results of SFE calculations, summarized in Tables 1 and 2 and illustrated in Figs. 1 and 2, were normalized by adjusting the value of the intercept to ~31 mJ/m^2 at 325 °C, reported by Latanision and Ruff [17] (for the composition of 10.7 wt% Ni–18.3 wt% Cr–0.005 wt% C).

Table 1
Summary of Bo and SFE results for in-reactor pressurized tubes

Alloy and heat	Temperature (°C)	Dose (dpa)	Reactor	Test	SFE (mJ/m^2)	Bo ($\times 10^{-6}$ MPa^{-1} dpa^{-1})	Reference
19Cr10Ni (SA T304L)	380–415	10	EBR-II	Creep I	15.3	0.5	[31] (Fig. 3) and this evaluation
17Cr14NiMo (HT V87210)	385–400	20			26.2		
10% CW T316		20	EBR-II	Creep II		0.9	[33] and this evaluation
20% CW T316		20	EBR-II	Creep II		1.1	[33] and this evaluation
18Cr14NiMo (HT 81581) 20% CW T316 (tube E245)		20	EBR-II	Creep II	26.0	1.6	This evaluation
18Cr14NiMo (FFTF fourth core) 20% CW T316		20	EBR-II	Creep II	23.8	1.4	This evaluation
18Cr14NiMo (HT 81581)					26.0		
20% CW T316 (beams)	380	15	EBR-II	C-1		1.3	[13] (Fig. 5)
20% CW T316 (tubes)	410	15	EBR-II	P-10		1.3	[34] (Fig. 1)
17Cr14NiMo	377	13	EBR-II	P-1	26.2	1.6	[34] (Fig. 2)
(HT V87210 N2 lot)	377	13	EBR-II	P-1		1.3	[25] (Fig. 1)
20% CW T316	377–410	7	EBR-II	P-1		1.4	[25] (Fig. 13)
		7	EBR-II	P-10		1.4	[25] (Fig. 13)
17Cr12NiMoCuNbTiS (HT X15893) 20% CW T316	330	12	ORR	–	36.9	2.3	[25] (Fig. 7)
14Cr16NiMoTi (SA JPCA)	330	7.4	ORR	–	30.7	1.6	[35]
17Cr14NiMoNb (20% CW J316)		7.4	ORR	–	22.8	1.3	[35]
Fe–13.5Cr–15Ni		7.4	ORR	–	46.4	3	[35]
14Cr16NiMoTi K280 (25% CW USPCA)	330	7	ORR	–	33.8	2.3	[28]
14Cr16NiMoTi (SA JPCA)		7	ORR	–	30.7	1.6	[28]

17Cr14NiMoNb (20% CW J316)	7	ORR	–	22.8	1.3	[28]
17Cr14NiMo HT 81600 (20% CW T316)	396–405	20	FFTF MOTA	24.6	1.5	[29] (Fig. 4)
		20	FFTF MOTA		1.1	[29] (Fig. 4)
		20	FFTF MOTA		1.3	[29] (Fig. 4)
		20	FFTF MOTA		1.4	[29] (Fig. 4)
		20	FFTF MOTA		1.4	[29] (Fig. 4)
14Cr17NiMoTi	386–405	100	FFTF MOTA	35.8	2.1	[35] (Table 1)
K280 20% CW PCA		100	FFTF MOTA		2.2	[35] (Table 1)
		100	FFTF MOTA		2.3	[35] (Table 1)
		100	FFTF MOTA		2.4	[35] (Table 1)
		100	FFTF MOTA		2.4	[35] (Table 1)
14Cr16NiMoTi	~420	45	PFR	25.4	1.1	[2] (Table 2)
HT 2966 (20% CW D9)					1.0	[2] (Table 2)
16Cr15NiMoNb (steel 1)	350 and 420	20	BOR-60	29.9	1.8	[36]
16Cr15NiMoNb (steel 2)		20	BOR-60	28.8	1.5	[36]

Fig. 1. Correlation of Bo with SFE for austenitic stainless steel pressurized tubes.

Both the transient irradiation creep component, A_1, and Bo are linearly dependent on the SFE. This conclusion is based on the relationship between the transient strain amplitude, A_1, and Bo illustrated in Fig. 4 of Garner and Toloczko [22] for helices, and the common mechanism of climb-enhanced dislocation glide for both the transient and Bo creep compliance terms [10]. Borodin and Ryazanov [9] indicate that both the transient irradiation creep and the Bo creep compliance are sensitive to jog formation, and hence, SFE. Tables 1 and 2 include both solution annealed (SA) and cold-worked (CW) irradiation creep data because there appears to be little difference in Bo for austenitic stainless steels in the solution annealed and various levels of cold work. Garner et al. [26] showed similar creep strains for 10, 20, and 30% CW for 316 SS pressurized tubes during irradiation at 400 °C in EBR-II. Little effect of CW on irradiation creep was found by Ehrlich [27]. Grossbeck et al. [28] investigated the effect of cold work for type 316 stainless steel and the PCA alloys. The Bo values for 316 SS in the SA and 20% CW conditions, and for the PCA alloy in the SA and the 25% CW conditions were observed to be similar. As a result, Grossbeck et al. [28] concluded that cold work did not affect the value of Bo.

The variation of the same materials tested in different reactors was generally comparable to the specimen-to-specimen variability for testing in the same reactor. In the case of the pressurized tubes, the consistency of dose calculations enabled Bo to be correlated with the SFE for tests conducted in five different reactors. The largest reactor-to-reactor variability in Bo was observed for pressurized tubes of 316 Heat 81600 irradiated in FFTF and PFR as reported by Garner et al. [29]. The reason for this variability is due to large uncertainty in the stress and temperature. The in-reactor creep results for 316 Heat 81600 were

Table 2
Summary of Bo and SFE results for helices irradiated in the DFR [23,24]

Alloy	Specimen	Test rig	Temperature (°C)	Dose (dpa)	SFE (mJ/m^2)	Bo ($\times 10^{-6}$ MPa^{-1} dpa^{-1})
17Cr14NiMoTiNb	1(3)	395	290–304	4.5	17.2	0.88
20% CW M316-1	4(3)		271–290	4.7		0.74
17Cr14NiMo	4(4)			3.9	19.6	1.19
20% CW M316-2	9(3)		247–290	4.6		1.13
17Cr13NiMo	6(2)		271–290	4.4	20.2	0.91
20% CW M316-3	7(2)					0.79
17Cr12NiMo	15(2)			4.0	18.6	0.85
20% CW M316-II						
17Cr12NiMoNb	4(2)			4.4	21.8	1.11
20% CW FV548-1	9(2)			4.7		1.45
	1(1)	546		3.1		1.22
	4(1)	442	500	2.7		1.53
	4(3)			4.7		1.50
17Cr11NiMoNb	14(2)	395	290	4.3	22.8	1.28
20% CW FV548-II						
18Cr9NiMoTi	6(3)		271–290	4.4	23.0	1.45
20% CW EN58B-1	10(4)			3.1		1.5
	15(1)		271	3.3		1.59
18Cr11NiMo	7(1)		271–290	3.6	31.3	2.86
20% CW EN58E-1	12(2)		271–304	4.6		2.92
17Cr9NiMo	7(3)		271–290	4.5	23.0	1.62
20% CW EN58J-1	12(3)		271–304	4.6		1.56
17Cr12NiMo	1(3)	456	271–290	3.0	21.5	1.45
EN58J-II						

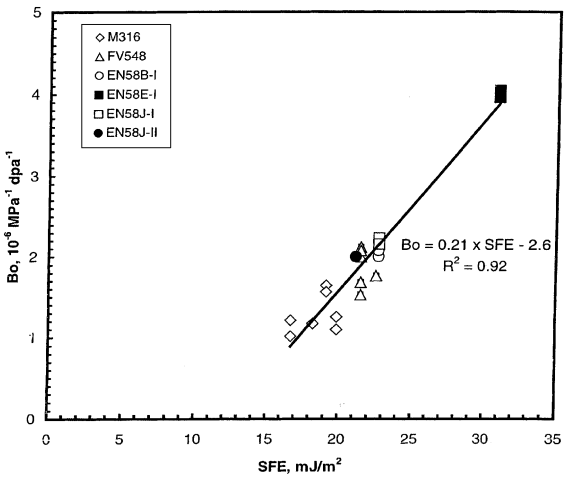

Fig. 2. Correlation between Bo and SFE for stainless steel springs irradiated in the Dounreay fast reactor.

obtained by irradiating pressurized tube specimens in high-flux and low-flux positions in the PFR De-mountable Subassembly (DMSA) vehicle. The temperature control in the DMSA is passive, i.e., not actively monitored. Analyses of the data were performed prior to receiving the coolant inlet and outlet temperatures. Without these details and estimates of the gamma heating, estimation of the uncertainties in the specimen temperatures was not possible. In-reactor creep is sensitive to both stress and temperature. Stress increases with increasing temperature of the test specimens. Calculated values of Bo for the low-flux specimens in the PFR ranged from 0.9 to 1.9×10^{-6} MPa^{-1} dpa^{-1}. Calculated values of Bo for the high-flux specimens in the PFR ranged from 2.8 to 3.1×10^{-6} MPa^{-1} dpa^{-1}. The values of Bo for the tubes irradiated under precisely controlled conditions in the FFTF ranged from 1.0 to 1.5×10^{-6} MPa^{-1} dpa^{-1} at 400 °C. Garner et al. [29] attributed the large variability in the Bo values obtained from the tests in the PRF to uncertainties in the test temperatures and stresses in the DMSA vehicle. These large uncertainties precluded using these PFR data for the correlation of Bo with the SFE.

Displacement dose calculations were performed for several of the pressurized tube irradiation creep tests to

confirm the consistency of the calculated Bo values. The displacement dose was calculated based on the axial location of each pressurized tube sample and the neutron flux shape. The neutron flux values were calculated with the two-dimensional solver routines in the transport code DANTSYS. These evaluations used the ENDF/B-V cross-sections and the sample radial–axial position geometry. The cross-sections were collapsed to a 28 energy group structure using weighting fluxes appropriate for specific regions in the EBR-II core (the fuel, reflector and blanket regions). The 28-group damage cross-sections were collapsed from ENDF/B-VI using the cross-section processing code NJOY. The calculated displacement-per-atom values were determined by multiplying the neutron fluence by the ENDF/B-VI damage cross-sections. The dpa and creep strains for 16 sibling 10% CW tubes in the Creep-II test in EBR-II were evaluated. The mean value of Bo was 0.86×10^{-6} MPa^{-1} dpa^{-1} with a standard deviation of 0.15×10^{-6} MPa^{-1} dpa^{-1}. This mean value for Bo is in good agreement with the average value of $\sim 0.9 \times 10^{-6}$ MPa^{-1} dpa^{-1} shown in Fig. 9 by Porter et al. [32], for data from the same in-reactor test. An evaluation of the creep strains for 13 sibling 20% CW tubes in the same Creep-II test resulted in a mean value of 1.06×10^{-6} MPa^{-1} dpa^{-1} for Bo. This mean value for Bo compares favorably with an average value of $\sim 1.2 \times 10^{-6}$ MPa^{-1} dpa^{-1} for tubes from the same test reported by Porter et al. [32]. An evaluation of the results from three pressurized tube creep tests with the FFTF Fourth Core 316 SS cladding in the Creep-II test in EBR-II resulted in an average value of 1.4×10^{-6} MPa^{-1} dpa^{-1} for Bo. An evaluation of 12-pressurized and 2-unstressed 304L SS tubes from the Creep-I test in EBR-II resulted in an average Bo value of 0.46×10^{-6} MPa^{-1} dpa^{-1}. This average result compares favorably with the zero fluence intercept value of $\sim 0.5 \times 10^{-6}$ MPa^{-1} dpa^{-1} shown in Fig. 3(b) by Porter et al. [31]. These results are included in Table 1.

Based on the correlation for Bo with composition developed by this investigation, austenitic stainless steel alloys can be identified and classified for low, medium, and high values of Bo. Based on Eq. (6), alloys with values of SFE as low as 6–8 mJ/m^2 [15,18,20] should have very low values of Bo. The available data are insufficient to determine the breaking point in the linearity of Eq. (6) at very low values of SFE. In-reactor creep data are not available to evaluate the extension of the linear Bo versus SFE correlation to alloys with very low values of SFE. Materials such as 316LN SS and 316FR SS [30] that contain N should be tested to verify the potential for N to reduce Bo. Other alloy constituents such as Ni can be adjusted to obtain the desired Bo. While additions of Ti, Nb, and Si solutes significantly reduce Bo, potential dilation due to the formation of solid-state precipitates from excessive additions may need to be taken into consideration.

5. Conclusions

The following conclusions may be reached based on the results presented above:

1. The dislocation SFE is an important parameter affecting the non-swelling component of in-reactor creep.
2. The compositional dependences of SFE, IGSCC, and pitting corrosion are similar to the composition dependence of the non-swelling component of creep.
3. The Ni content of austenitic stainless steel has opposite effects on swelling and the non-swelling component of creep.
4. In-reactor creep data and irradiation creep theory indicate that the transient irradiation creep and Bo are similarly affected by the SFE.
5. Alloys with a wide range of SFE (compositions) should be characterized and tested to provide improved understanding of the effect of SFE on the non-swelling components of in-reactor creep. For applications requiring low values of Bo, austenitic stainless steels such as 316LN and 316FR containing nitrogen should be characterized for SFE and in-reactor creep behavior.

References

[1] F.A. Garner, in: B.R.T. Frost (Ed.), Materials Science and Technology, Vol. 10A Nuclear Materials Part 1, VCH, Germany, 1994 (Chapter 6).
[2] M.B. Toloczko, F.A. Garner, J. Standring, B. Monro, S. Adaway, J. Nucl. Mater. 258–263 (1998) 1606.
[3] J.F. Bates, R.W. Powell, E.R. Gilbert, in: Effects of Radiation on Materials: 10th Conference, ASTM STP-725, 1981, p. 713.
[4] H. Hausen, W. Schule, in: Effects of Radiation on Materials: 18th International Symposium, ASTM STP 1325, 1999, p. 830.
[5] H. Hausen, W. Schule, in: Effects of Radiation on Materials: 18th International Symposium, ASTM STP 1325, 1999, p. 742.
[6] W.G. Wolfer, J. Nucl. Mater. 90 (1980) 175.
[7] S. Jitsukawa, Y. Katano, K. Shiraishi, J. Nucl. Sci. Technol. 2 (1984) 671.
[8] S. Jitsukawa, Y. Katano, K. Shiraishi, F.A. Garner, in: Effects of Radiation on Materials: 15th International Symposium, ASTM STP 1125, 1992, p. 1034.
[9] V.A. Borodin, A.I. Ryazanov, in: Effects of Radiation on Materials: 15th International Symposium, ASTM STP 1125, 1992, p. 530.
[10] R.E. Stoller, M.L. Grossbeck, L.K. Mansur, in: Effects of Radiation on Materials: 15th International Symposium, ASTM STP 1125, 1992, p. 517.
[11] C.H. Woo, F.A. Garner, J. Nucl. Mater. 233–237 (1996) 974.
[12] F.A. Garner, T. Lauritzen, M.A. Mitchell, in: Effects of Radiation on Materials: 16th International Symposium, ASTM STP 1175, 1993, p. 803.

[13] J.P. Foster, E.R. Gilbert, K. Bunde, D.L. Porter, J. Nucl. Mater. 252 (1998) 89.
[14] P.J. Brofman, G.S. Ansell, Metall. Trans. A 9A (1978) 879.
[15] R.E. Schramm, R.P. Reed, Metall. Trans. A 6A (1975) 1345.
[16] P.J.C. Gallagher, Metall. Trans. 1 (1970) 2429.
[17] R.M. Latanision, A.W. Ruff Jr., Metall. Trans. 2 (1971) 505.
[18] D.L. Douglas, G. Thomas, W.R. Roser, Corrosion 20 (1964) 15t.
[19] J.C. Li, W. Zheng, Q. Jiang, Mater. Lett. 38 (1999) 275.
[20] P.R. Swann, Corrosion 19 (1963) 102t.
[21] R.F.A. Jargelius-Petterson, Corrosion 54 (1998) 162.
[22] F.A. Garner, M.B. Toloczko, J. Nucl. Mater. 251 (1997) 252.
[23] G.W. Lewthwaite, D. Mosedale, J. Nucl. Mater. 90 (1980) 205.
[24] D. Mosedale, G.W. Lewthwaite, in: Proc. Iron and Steel Institute Conference on Creep Strength in Steel and High-Temperature Alloys, Sheffield, UK, 1972, p. 169.
[25] J.P. Foster, K. Bunde, M.L. Grossbeck, E.R. Gilbert, J. Nucl. Mater. 270 (1999) 357.
[26] F.A. Garner, M.L. Hamilton, C.R. Eiholzer, M.B. Toloczko, A.S. Kumar, in: Effects of Radiation on Materials: 16th International Symposium, ASTM STP 1175, 1993, p. 696.
[27] K. Ehrlich, J. Nucl. Mater. 100 (1981) 149.
[28] M.L. Grossbeck, L.T. Gilbson, S. Jitsukawa, L.K. Mansur, L. Turner, in: Effects of Radiation on Materials: 18th Conference, ASTM STP 1325, 1999, p. 725.
[29] F.A. Garner, M.B. Toloczko, B. Munro, S. Adaway, J. Standring, in: Effects of Radiation on Materials: 18th Conference, ASTM STP 1325, 1999, p. 713.
[30] C.R. Brinkman, in: Advances in Life Prediction Methodology, ASME PVP-391, 1999, p. 87.
[31] D.L. Porter, G.D. Hudman, F.A. Garner, J. Nucl. Mater. 179–181 (1991) 581.
[32] D.L. Porter, E.L. Wood, F.A. Garner, in: Effects of Radiation on Materials: 14th International Symposium, ASTM STP 1046, 1990, p. 551.
[33] J.P. Foster, K. Bunde, E.R. Gilbert, J. Nucl. Mater. 257 (1998) 118.
[34] M.L. Grossbeck, L.T. Gibson, S. Jitsukawa, J. Nucl. Mater. 233–237 (1996) 148.
[35] M.B. Toloczko, F.A. Garner, C.R. Eiholzer, J. Nucl. Mater. 191–194 (1992) 803.
[36] V.S. Neustroev, V.K. Shamardin, in: Effects of Radiation on Materials: 16th International Symposium, ASTM STP 1175, 1993, p. 816.